Lasers in Manufacturing Conference 2023

Automated weld seam evaluation and 2D simulation parameter calibration for absorber-free laser transmission welding

Frederik Maiwald*, Johannes Tröger, Stefan Hierl

Laser Material Processing Laboratory, Ostbayerische Technische Hochschule Regensburg, Am Campus 1, 92331 Parsberg, Germany

Abstract

Absorber-free laser transmission welding enables clean and precise joining of plastics without additives or adhesives. It is therefore well suited to produce optical and medical devices, which place high demands on cleanliness and accuracy. However, the weld usually has an undesirably large vertical expansion, causing bulges and distortion. To improve this, the intensity distribution of the laser beam as well as the processing strategy must be adapted. Due to the complexity, this is aided by process simulation. However, simulation parameter calibration and verification are usually done considering the seam width and height, which is of limited significance. To overcome this, we propose a new method for image processing of microtome sections, determining the spatially resolved geometry of the weld. Thus, the deviation between experiment and simulation can be calculated pixel by pixel. This spatially resolved value is predestined for the calibration of the simulation parameters: For a parameter field with 18 different settings, the total deviation between experiment and simulation is less than 11 % after calibration.

Keywords: plastics welding; image processing; simulation; optimization

1. Introduction

Absorber-free laser transmission welding is a favored joining process in medical industry, enabling clean and precise joining of plastics without additives or adhesives. Figure 1 shows the principle of absorber-free laser transmission welding. Both joining partners are clamped in an overlap. A laser beam with its wavelength in the polymers' intrinsic absorption spectrum between 1.6 µm and 2.1 µm is focused with comparably high numerical aperture (NA) inside of the sample. The intensity gradients generated in this way enable selective

* Corresponding author. Tel.: +49 9492/8384-108.
E-mail address: frederik.maiwald@oth-regensburg.de

fusion of the joining zone without affecting the outer surfaces, even without external cooling [1–6]. However, the ratio of weld width divided by weld height is small, since the weld seams are high in the vertical, but narrow in the horizontal direction. This is a disadvantage, because certain weld width requirements to ensure strength or tightness, can only be fulfilled to a limited extent. The seam quickly becomes too large in the vertical direction, resulting in visible and noticeable bulges [5–11].

To increase the aspect ratio, i.e. to create a wider seam with the same seam height, several seams can be placed next to each other [5] or external cooling can be used [12, 13]. Alternatively, beam superposition [6, 8, 9] or adapted – non-gaussian – intensity distributions are used to directly generate the improved weld seam geometry (figure 1 (b)). Process simulations are performed to design the process, taking into account beam shaping, repetition rates, material properties as well as external cooling [1, 3, 4, 14, 15]. Due to measurement inaccuracies and assumptions in the input variables, the simulation parameters must be calibrated by matching experiment and simulation. Therefore, microtome sections are prepared and weld seam height (*h*) and width (*w*) are measured.

By using adapted beam shapes and process strategies, weld seam geometries deviating from the usual elliptical shape can be produced (figure 1 (b)). Considering only weld width and height, the comparison of experiment and simulation is only possible to a limited extent. To overcome this problem and enable the comparison of arbitrary welds, this work proposes a new method for spatially resolved, pixel-by-pixel acquisition and comparison of weld seam geometries. Image processing is used to identify and digitize the weld seam geometry automatically in photographs of microtome sections. After a statistical evaluation of the seams, it is compared with the simulation results in a spatially resolved manner. The total error is used as an objective to calibrate the parameters of the process simulation and minimize the difference between simulation and experiment.

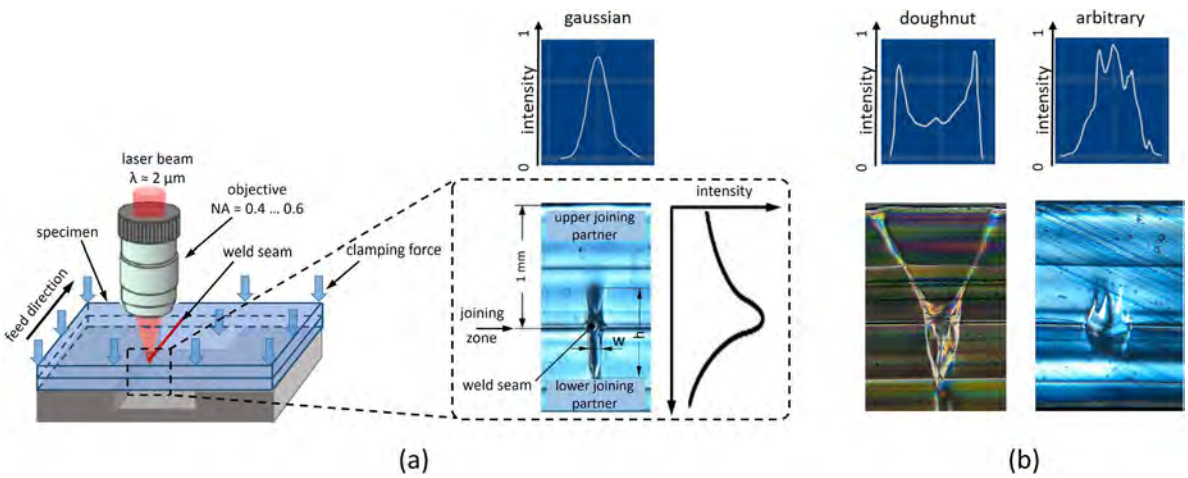

Fig. 1. (a) Sketch of the experimental setup for absorber-free laser transmission welding (adapted from [19]). The microtome section on the right shows an elliptic weld seam geometry produced with a gaussian beam. (b) Welds with non-elliptic geometry produced by non-gaussian beams. The measurement result of the respective intensity distribution is shown above the photos of the microtome sections (Material: Ultramid b3s). The horizontal lines outside the joining zone result from the injection molding process of the plates and from the knife of the microtome.

2. Materials and methods

2.1. Samples

Semi-crystalline polyamide (Ultramid b3s, BASF SE) was used for the welding tests. Plates with 50x50x1.05 mm³ were produced by injection molding and strips of 10 mm width were cut from these plates. Using an integrating sphere, the transmittance T (20 %) and reflectance R (4 %) were measured at a wavelength of 1940 nm. Considering the sample thickness of 1.05 mm, the coefficient of absorption α = 0.8 mm^{-1} was calculated. Figure 2 depicts the thermal conductivity λ measured by the xenon flash method according to ISO22007-4 and the heat capacity c_p measured by the differential scanning calorimetry according to ISO 11357-4.

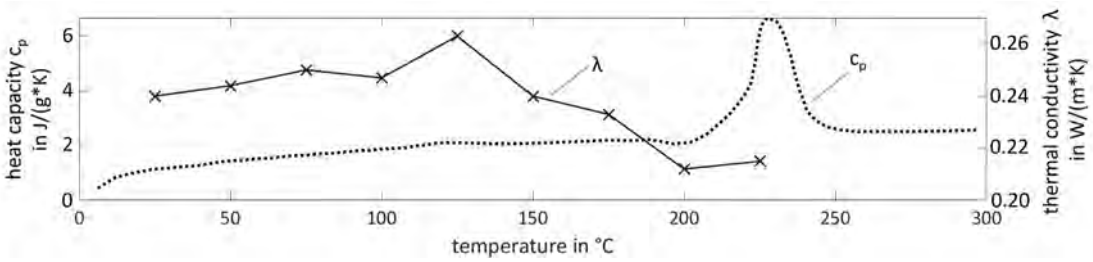

Fig. 2. Heat capacity (dotted line) und thermal conductivity (-X- line) of PA6 (Ultramid b3s) in dependence on temperature.

2.2. Experimental setup and processing parameters

Figure 1 shows the experimental setup, which has already been presented in earlier work [4]. It consists of a thulium fiber laser (λ = 1940 nm, TLR-120-WC-Y12, IPG Laser GmbH, Burbach, Germany) with maximum 120 W (cw) power. The raw beam can be expanded with an adjustable beam expander with magnification from 1x to 3x. After expansion, the beam propagates through a Galilean telescope, which focuses the beam with a focal length of 35 mm. All optics are mounted on a rail that is moved with 0.01 mm accuracy, enabling the adjustment of the laser focus position inside the part being processed. The specimens are clamped in overlap and fixed by a clamping goggle with clamping screws. The clamping goggle with the samples is moved by an axis system.

By adjustment of the beam expander, the NA was set to 0.5. The welds were processed with 200 mm/s feed rate between 0.14 J/mm and 0.46 J/mm energy per unit length (E). Three different laser focus positions z_{focus} of 1.0 mm, 1.1 mm, and 1.2 mm were used. The value of z_{focus} = 1.0 mm equals a focus position in the joining zone. For every parameter setting, one sample strip containing at least six weld seams was manufactured.

2.3. Weld seam analysis

After welding, 35 µm to 60 µm thick microtome sections of the specimens are produced using a rotary microtome (Leica RM2255, Leica Microsystems Ltd.). The sections are subsequently digitized in polarized light using a digital camera attached to a transmitted light microscope (see fig. 3 (a)). Due to melting and resolidification, the weld seam has different optical properties than the base material and can be identified.

3. Automated weld seam identification and evaluation

The weld seam visible in the images of the microtome sections can be measured by hand. However, the manual procedure is time-consuming for a large number of welds and the result depends on the operator. Therefore, a method for automated identification of the weld seam was developed.

3.1. Weld seam identification

Figure 3 shows the steps of automated weld seam identification using macros in Fiji/ImageJ [16, 17] . After importing the photographs of the microtome sections (see figure 3 (a)), the horizontal lines resulting from the injection molding process of the plates are removed first. Thus, the 1st derivative of the image in horizontal x-direction is calculated using the "*FeatureJ Derivatives*"-algorithm [18]. Figure 3 (b) shows the resulting gradient image, where the horizontal lines are eliminated. Subsequently, the boundary between weld seam and base material is detected: First, edge detection using the *"Canny Edge"*-algorithm [19, 20] is performed, but the identified boundary remains rugged and contains artifacts (see figure 4 (c)). To improve this, fragments below the size of 2 000 pixels (4 µm²) are discarded using the *"Find Connected Regions"*-algorithm, resulting in a closed weld contour (see figure 3 (d)). The resulting contour is then filled using the *"Fill Holes"*-algorithm and the image is binarized. In figure 3 (e), white color corresponds to the weld seam and black color to the base material. As figure 3 (d) demonstrates, the detected contour (red) coincides well with the actual contour of the weld seam.

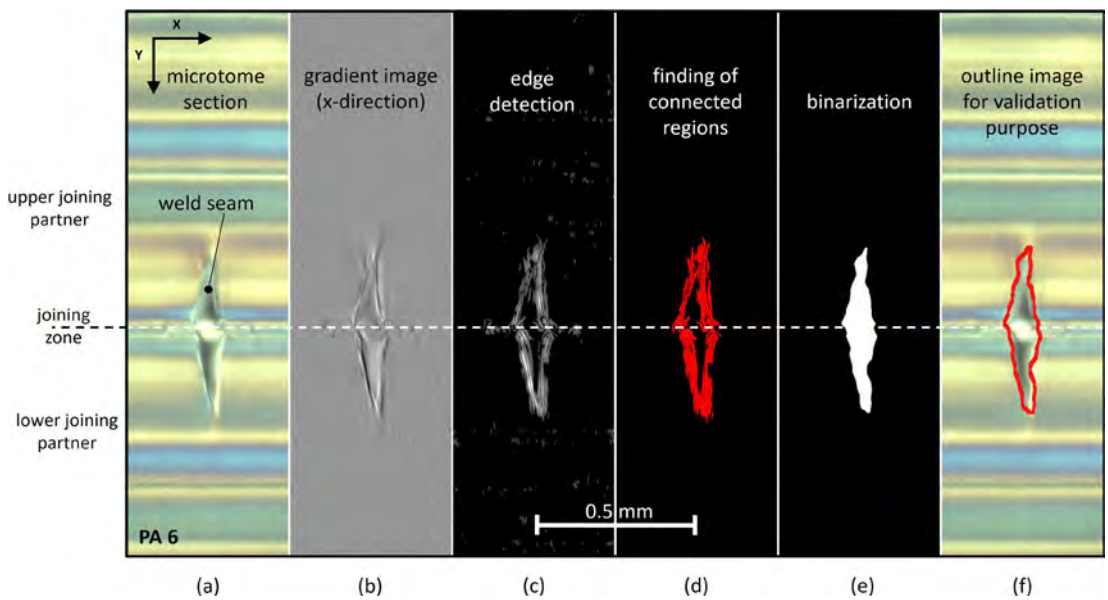

Fig. 3. (a) Microtome section of a specimen made of polyamide (Ultramid b3s) photographed in polarized transmitted light; (b) Visualization of the first derivation of the image in X-direction; (c) Image after application of edge detection and after (d) filtering; (c) Binary image with the weld in white and the base material in black and (f) comparison of the identified seam and the original image.

3.2. Weld seam evaluation

After weld seam identification, statistical evaluation is performed. Figure 4 illustrates the evaluation procedure using two welds. Their position in vertical y-direction is already defined since the top of the specimen has been aligned to the top of the image during photography. To enable alignment in horizontal x-direction, the x-centroid is calculated (see vertical red and blue line figure 4 (a, b)). After alignment, the frequency with which a pixel belongs to the weld seam is calculated. Figure 4 (c) shows the resulting grayscale image, where the grayscale value of a pixel can be 0, 50 or 100: With a value of 0, the pixel was never part of the weld seam. At 50, in one of two images the pixel was identified as weld seam and at 100 in both images.

Since both the welding setup and the specimen are symmetrical, the seam is expected to be symmetrical as well. Deviations from symmetry are considered statistical errors due to e.g., inhomogeneous material, alignment issues or surface defects. To implement symmetry in the weld seam analysis, the binary images (a) and (b) are mirrored along the X-centroid. After alignment of the initial and the mirrored images, the frequency with which a weld is present is calculated pixelwise. Figure 4 (d) shows the resulting grayscale image. Compared to (c), (d) it is symmetrical and has more grayscale values.

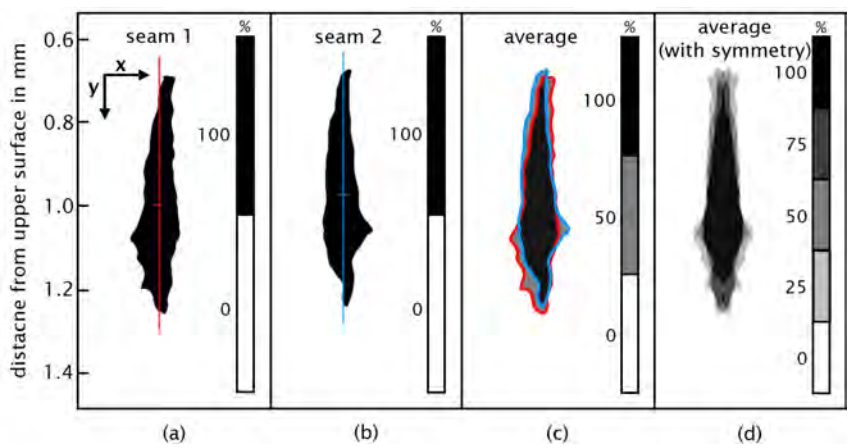

Fig. 4. (a, b) Two weld seams with sketched x-centroid as well as (c) their superposition; (d) Grayscale image calculated from superposition of weld seams with symmetry taken into account. The darker the color, the more likely a weld is present locally.

4. Process model and parameter calibration

4.1. Process Model

To compute the temporal and spatial temperature course during processing, a thermal finite element analysis is set up in COMSOL Multiphysics (see figure 5). The volumetric heat source is implemented as already presented in previous work [4]. Due to symmetry of the experimental setup, only a half model is realized. Material properties are implemented according to chapter 2.1 and process parameters according to chapter 2.2. Due to the high feed rate of 200 mm/s and the low thermal conductivity of the polymer, heat flow in feed direction can be neglected and a two-dimensional model is established. Due to calculation's complexity and lengthy computing time, the temperature dependency of the coefficient of absorption [21] and of the refractive index [22] is neglected. The influence of the high heating and cooling rates on the melting and crystallization behavior [23–25] is neglected, too. The reduced thermal conductivity between both joining

partners is neglected and both partners are modeled as one. This is possible, since both joining partners are heated mainly by absorption of the laser beam. Unlike in transparent-absorbent welding, where the upper joining partner is mainly heated by heat conduction from the lower one and the reduced thermal conductivity should be considered [26–28].

To derive the weld seam geometry from the computed temperature field, the maximum temperature during the entire process is determined for every element. Each element that has once exceeded the melting temperature T_{melt} is assigned to the weld.

Finally, the computed and the experimentally determined weld seam geometry are compared pixel by pixel (see figure 5 (b)). The pixelwise probability of weld seam occurrence as determined in chapter 3 is used as experimental data. The error per pixel can be between -100 % and +100 %: Cyan means that simulation and experiment match. The error is 0. Yellow (error = +100 %) means that the simulation does not predict a weld, but there was a weld in every experiment. A greenish tint corresponds to +50 % error: This means that no seam was predicted, but in the experiment, a weld was present in 5 out of 10 trials. Blue represents -100 % error: Here, the simulation predicts a weld but there never was one in the experiment. Finally, the total error is calculated as residual sum of squares over all pixels.

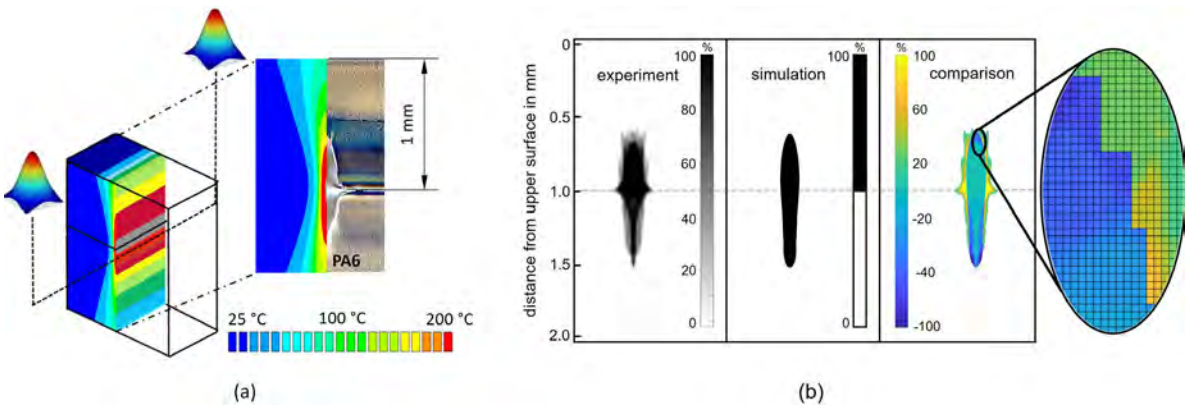

Fig. 5. (a) Computed maximum temperatures after processing and comparison of temperature and related weld seam in a microtome section. (b) Comparison of experimental and computed seam. In the magnified image on the right, negative values (yellow) indicate that a weld is present in the experiment but not in the simulation. Positive values (blue) indicate that a weld was predicted but is not present in the experiment. Cyan and white indicate, that experiment and simulation match.

4.2. Simulation parameter calibration

The measurement of the process parameters is subject to inaccuracies, and their value inside the sample can only be determined indirectly. To compensate the resulting inaccuracies with acceptable effort in computation and measurement, simulation parameter calibration is required. Table 1 shows the implemented parameters with their confidence intervals. The angle of convergence inside the polymer ϑ_{poly} and consequently the focal beam diameter and the laser focus position $z_{focus,\ poly}$ are affected by surface refraction. It was determined by analyzing small welds, that a focus shift of 0.1 mm in air results in 0.15 mm shift in plastic. This factor is denoted K_{focus}. Furthermore, the focus position $z_{focus,\ poly}$ = 1.0 mm does not correspond exactly to the joining zone. The deviation is designated as Δz_{focus}. By the beam quality factor M^2, both aberrations, caused by imperfections and misalignment of the optical system including the component surface, are considered. Scattering of the laser beam [29–31] is neglected. The focus diameter was measured in air to be 35 µm, which is already more than 10 times larger than the theoretical diameter of 2.34 µm. In the energy per unit length, deviation of ±7.5% laser power, ±2.5 % reflection (caused by surface roughness and angle of incidence) and

±12.5 % feed rate is combined to a total deviation of ±15 % using a quadratic tolerance calculation. After parameter definition, the weld seam geometries were fully factorially calculated and the setting with the smallest deviation between all 18 experimental parameter settings and simulation was determined.

Table 1. Confidence intervals of the parameters for simulation parameter calibration as well as the optimum setting.

Abbrev.	Parameter	Unit	Min.	Max.	Optimum	step
ϑ_{poly}	angle of convergence in polymer	°	15	24	24	3
M^2	beam quality	-	15	45	35	5
K_{focus}	magnification of focus shift	-	1.2	1.35	1.5	0.05
Δz_{focus}	deviation of laser focus position	mm	-0.04	0.04	0.02	0.02
α	coefficient of absorption	1/mm	0.78	0.89	0.83	0.045
T_{melt}	melting temperature	°C	220	250	235	5°C
E_{err}	energy per unit length (relative error)	%	-10	+10	-10	10

5. Results and experimental verification

Figure 6 shows the result of the simulation parameter calibration performed with the optimum parameter set given in table 1 in comparison with the experimental result. In the center row (z_{focus} = 1.10 mm), the computed welds are outlined in red for clarity. The area of all 18 experimental weld seams is 1.31 mm² and the total error after calibration is 0.14 mm². This corresponds to a relative deviation of less than 11 %. The computed result coincides well with the experiment for the entire parameter field.

Close to the joining zone, the experimental welds are always wider than the computed ones. This is due to melt flow into the gap between both joining partners, which is neglected in the simulation. However, melt squeeze out is an indication of insufficient contact due to low clamping pressure and must be avoided, since the melt can for example block fluid channels in application. Since the total error is used for calibration, large welds (with high energy per unit length) have a bigger influence on the result than small ones. A fundamental problem of simulation parameter calibration is that an erroneous parameter can be compensated by the unreasonable adjustment of another. For example, the weld size is influenced by the energy per unit energy, the coefficient of absorption and the temperature T_{melt}. Care must be taken that confidence intervals are as large as necessary but as small as possible.

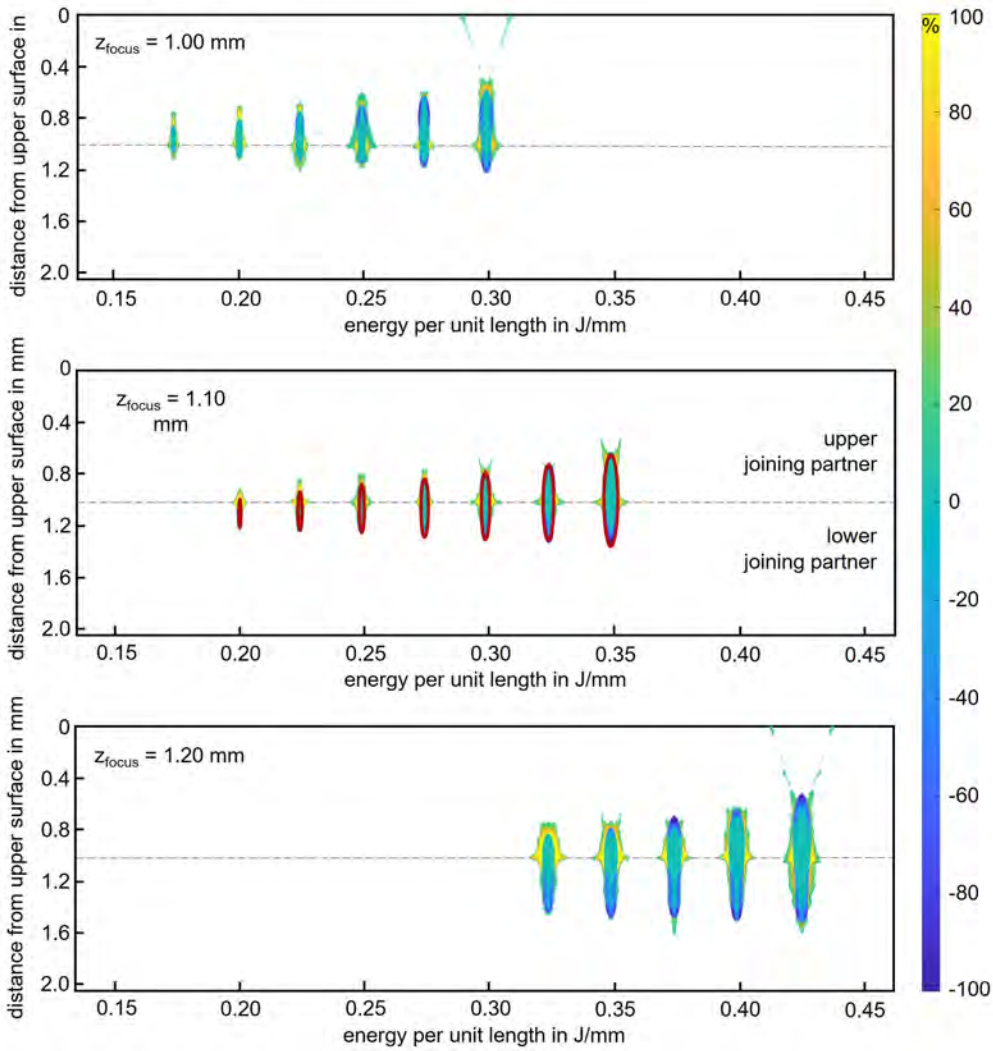

Fig. 6. Comparison of experimental and computed weld seam geometry in dependence on energy per unit length for three laser focus positions (parameters as shown in Table 1). In the center row (z_{focus} =1.10 mm), the computed welds are outlined in red for clarity. Cyan and white indicate, that experiment and simulation match. Negative values (yellow) indicate that a weld was present in the experiment but not in the simulation. Positive values (blue) indicate that a weld was predicted but was not present in the experiment.

6. Conclusion and outlook

In this work, a new approach for spatially resolved weld seam analysis in absorber-free laser transmission welding is presented. The seam is automatically identified by image processing and the probability of each pixel belonging to the weld seam or to the base material is calculated. This spatially resolved value is predestined for the calibration of the simulation parameters. As demonstrated in this work, this ensures a good agreement with less than 11 % deviation between calculated and experimentally determined seams.

In future work, the algorithm for identifying the optimal parameters will be optimized to save computation time and the method will be used for different materials. To reduce the confidence intervals of the input

parameters, further measurements are scheduled. The calibrated simulation will then be used to evaluate adapted laser beam shapes and processing strategies for improved weld geometries. Additionally, the method for spatially resolved weld seam analysis will be used for weld seam analysis in industrial parts and an assessment of the process stability.

Acknowledgements

The results presented in this publication were obtained within the project "Absorberfreies Laser-Kunststoffschweißen für qualitätskritische High-Volume-Anwendungen in der Medizintechnik (CTC-Med)", which was funded by the Bavarian Research Foundation (AZ-1519-21). The authors gratefully thank the project partner Evosys Laser GmbH, AdlOptica Optical Systems GmbH and Gerresheimer Regensburg GmbH for technical discussion and for providing samples. We personally thank F. Fries, L. Koller, P. Wiesner and S. Piskurek for assistance in the installation of the experimental setup as well as execution of experiments.

References

[1] ADEN, Mirko; GILLNER, Arnold; OTTO, Gerhard; MAMUSCHIK, Viktor: Laserdurchstrahlschweißen transparenter Kunststoffe Teil 1: Betrachtung des Energieeintrags. In: Kunststoffe (2018), 3/4

[2] OLOWINSKY, Alexander; OTTO, Gerhard; JANZEN, Roland; MAMUSCHKIN, Viktor: Laserdurchstrahlschweißen transparenter Kunststoffe – Teil 2: Schweißen von PC mit 1940 nm Laserstrahlung: Laser transmission welding of transparent plastics – Part 2: Welding of PC with 1,940 nm laser radiation. In: JOINING PLASTICS 2019

[3] MAIWALD, Frederik; ENGLMAIER, Stephan; HIERL, Stefan: Online Pyrometry for Weld Seam Localization in Absorber-Free Laser Transmission Welding of Transparent Polymers. In: Journal of Laser Micro/Nanoengineering (2021)

[4] MAIWALD, Frederik; ENGLMAIER, Stephan; HIERL, Stefan: Absorber-free laser transmission welding of transparent polymers using fixed focus optics and 3D laser scanner. In: Procedia CIRP 94 (2020), S. 686–690

[5] NGUYEN, Nam-Phong; BROSDA, Maximilian; OLOWINSKY, Alexander; GILLNER, Arnold: Absorber-Free Quasi-Simultaneous Laser Welding For Microfluidic Applications. In: Journal of Laser Micro/Nanoengineering (2019)

[6] POLSTER, Steffen: Laserdurchstrahlschweißen transparenter Polymerbauteile. Friedrich-Alexander-Universität Erlangen-Nürnberg. Doctoral Thesis. 2009

[7] NGUYEN, Nam-Phong; BEHRENS, Stefan; BROSDA, Maximilian; OLOWINSKY, Alexander; GILLNER, Arnold: Laser transmission welding of absorber-free semi-crystalline polypropylene by using a quasi-simultaneous irradiation strategy. In: Welding in the World 64 (2020), Nr. 7, S. 1227–1235

[8] MAMUSCHKIN, Viktor; OLOWINSKY, Alexander; VAN DER STRAETEN, Kira; ENGELMANN, Christoph: Laser transmission welding of absorber-free thermoplastics using dynamic beam superposition. In: DORSCH, Friedhelm (Hrsg.): High-Power Laser Materials Processing: Lasers, Beam Delivery, Diagnostics, and Applications IV : SPIE, 2015 (SPIE Proceedings), 93560Y

[9] MAMUSCHKIN, Viktor; ENGELMANN, Christoph; OLOWINSKY, Alexander: Improvement of Energy Deposition in Absorber-free Laser Welding through Quasi-simultaneous Irradiation. In: Physics Procedia 83 (2016), S. 472–482

[10] MAIWALD, Frederik; ROIDER, Clemens; SCHMIDT, Michael; HIERL, Stefan: Optical Coherence Tomography for 3D Weld Seam Localization in Absorber-Free Laser Transmission Welding. In: Applied Sciences 12 (2022), Nr. 5, S. 2718

[11] MINGAREEV, Ilya; WEIRAUCH, Fabian; OLOWINSKY, Alexander; SHAH, Lawrence; KADWANI, Pankaj; RICHARDSON, Martin: Welding of polymers using a 2µm thulium fiber laser. In: Optics & Laser Technology 44 (2012), Nr. 7, S. 2095–2099

[12] KUROSAKI, Yasuo; SATOH, Kimitoshi: A fiber laser welding of plastics assisted by transparent solid heat sink to prevent the surface thermal damages. In: Physics Procedia 5 (2010), S. 173–181

[13] DEVRIENT, M.; FRICK, T.; SCHMIDT, M.: Laser transmission welding of optical transparent thermoplastics. In: Physics Procedia 12 (2011), S. 157–165

[14] BROSDA, Maximilian; NGUYEN, Phong; OLOWINSKY, Alexander; GILLNER, Arnold: Analysis of the interaction process during laser transmission welding of multilayer polymer films with adapted laser wavelength by numerical simulation and thermography. In: Journal of Laser Applications 32 (2020), Nr. 2, S. 22060

[15] NGUYEN, Nam-Phong; BEHRENS, Stefan; BROSDA, Maximilian; OLOWINSKY, Alexander; GILLNER, Arnold: Modelling and thermal simulation of absorber-free quasi-simultaneous laser welding of transparent plastics. In: Welding in the World 64 (2020), Nr. 11, S. 1939–1946

[16] SCHINDELIN, Johannes; ARGANDA-CARRERAS, Ignacio; FRISE, Erwin; KAYNIG, Verena; LONGAIR, Mark; PIETZSCH, Tobias; PREIBISCH, Stephan; RUEDEN, Curtis; SAALFELD, Stephan; SCHMID, Benjamin; TINEVEZ, Jean-Yves; WHITE, Daniel James; HARTENSTEIN, Volker; ELICEIRI, Kevin; TOMANCAK, Pavel; CARDONA, Albert: Fiji: an open-source platform for biological-image analysis. In: Nature methods 9 (2012), Nr. 7, S. 676–682

[17] SCHNEIDER, Caroline A.; RASBAND, Wayne S.; ELICEIRI, Kevin W.: NIH Image to ImageJ: 25 years of image analysis. In: Nature methods 9 (2012), Nr. 7, S. 671–675

[18] MEIJERING, Erik: FeatureJ: An ImageJ Plugin Suite for Image Feature Extraction. URL http://imagescience.org/meijering/software/featurej/

[19] OLLION, Jean; COCHENNEC, Julien; LOLL, François; ESCUDÉ, Christophe; BOUDIER, Thomas: TANGO: a generic tool for high-throughput 3D image analysis for studying nuclear organization. In: Bioinformatics 29 (2013), Nr. 14, S. 1840–1841

[20] GERTYCH, Arkadiusz; MA, Zhaoxuan; TAJBAKHSH, Jian; VELÁSQUEZ-VACCA, Adriana; KNUDSEN, Beatrice S.: Rapid 3-D delineation of cell nuclei for high-content screening platforms. In: Computers in biology and medicine 69 (2016), S. 328–338

[21] GEIGER, M.; FRICK, T.; SCHMIDT, M.: Optical properties of plastics and their role for the modelling of the laser transmission welding process. In: Production Engineering 3 (2009), Nr. 1, S. 49–55

[22] CARIOU, J. M.; DUGAS, J.; MARTIN, L.; MICHEL, P.: Refractive-index variations with temperature of PMMA and polycarbonate. In: Applied optics 25 (1986), Nr. 3, S. 334–336

[23] RUSSEK, Ulrich Andreas: Prozesstechnische Aspekte des Laserdurchstrahlschweißens von Thermoplasten. RWTH Aachen University. Doctoral Thesis. 2006

[24] RÖHRICHT, M.-L.; STICHEL, T.; ROTH, S.; BRÄUER, P.A.B.; SCHMIDT, M.; WILL, S.: Correlation between weld seam morphology and mechanical properties in laser transmission welding of polypropylene. In: Procedia CIRP 94 (2020), S. 691–696.

[25] GEIßLER, Bastian; LAUMER, Tobias; WÜBBEKE, Andrea; LAKEMEYER, Patrick; FRICK, Thomas; SCHÖPPNER, Volker; SCHMIDT, Michael: Analysis of the interaction between the temperature field and the weld seam morphology in laser transmission welding by using two different discrete laser wavelengths. In: Journal of Laser Applications 30 (2018), Nr. 3, S. 32408

[26] SCHMAILZL, Anton; GEIßLER, Bastian; MAIWALD, Frederik; LAUMER, Tobias; SCHMIDT, Michael; HIERL, Stefan: Transformation of Weld Seam Geometry in Laser Transmission Welding by Using an Additional Integrated Thulium Fiber Laser. In: Lasers in Manufacturing (2017), S. 1–10

[27] LIU, Huixia; LIU, Wei; MENG, Dongdong; WANG, Xiao: Simulation and experimental study of laser transmission welding considering the influence of interfacial contact status. In: Materials & Design 92 (2016), S. 246–260

[28] WANG, Chuanyang; LIU, Haihua; CHEN, Zailiang; ZHAO, Dong; WANG, Chengdong: A new finite element model accounting for thermal contact conductance in laser transmission welding of thermoplastics. In: Infrared Physics & Technology 112 (2021), S. 103598

[29] ADEN, Mirko: Influence of the Laser-Beam Distribution on the Seam Dimensions for Laser-Transmission Welding: A Simulative Approach. In: Lasers in Manufacturing and Materials Processing 3 (2016), Nr. 2, S. 100–110

[30] ADEN, Mirko; MAMUSCHKIN, Viktor; OLOWINSKY, Alexander; GLASER, Sibylle: Influence of titanium dioxide pigments on the optical properties of polycarbonate and polypropylene for diode laser wavelengths. In: Journal of Applied Polymer Science 131 (2014)

[31] ADEN, Mirko; ROESNER, Andreas; OLOWINSKY, Alexander: Optical characterization of polycarbonate: Influence of additives on optical properties. In: Journal of Polymer Science Part B: Polymer Physics 48 (2010), Nr. 4, S. 451–455